Journal of Nanofluids
Vol. 10, pp. 408–419, 2021
(www.aspbs.com/jon)

ARTICLE

Three-Dimensional Rotating Flow of an Oldroyd-B Nanofluid with Relaxation-Retardation Viscous Dissipation

Manoj K. Nayak[1], Ibukun S. Oyelakin[2], Ali J. Chamkha[3], Sabyasachi Mondal[4,*], and Precious Sibanda[5]

[1]*Department of Mechanical Engineering, FET, ITER, Siksha O Anusandhan, Bhubaneswar 751030, Odisha, India*
[2]*School of Computer Science and Applied Mathematics, University of the Witwatersrand, Johannesburg, Private Bag 3, Braamfontein, 2050, South Africa*
[3]*Faculty of Engineering, Kuwait College of Science and Technology, Doha District, 35004, Kuwait*
[4]*Department of Mathematics, Amity University, Kolkata, Newtown 700135, West Bengal, India*
[5]*School of Mathematics, Statistics and Computer Science, University of KwaZulu-Natal, Private Bag X01, Scottsville, Pietermaritzburg, 3209, South Africa*

The principal aim of this study is to explore the impact of relaxation-retardation viscous dissipation, nonlinear convection, variable chemical reaction, and nonlinear thermal radiation on the three-dimensional rotating flow of an Oldroyd-B nanofluid over an exponentially extended surface. The Buongiorno model that takes into account the Brownian movement and thermophoresis responsible for nanoparticle motion. Exponentially varying temperature and concentration associated with convective heat transfer coefficients are assumed in the boundary conditions. The system of dimensionless ODEs is solved by the spectral quasi-linearization method. The results of the analysis show, among other results that the relaxation time parameter opposes the momentum transport while assisting heat transportation. The retardation time parameter acts to support momentum growth while reducing and resists heat transport. The present study focused on the investigation the effect of relaxation and retardation viscous dissipation on rotating flow of a non-Newtonian fluid (Oldroyd B fluid) past an exponential stretching sheet.

KEYWORDS: Rotating Flow, Oldroyd B Nanofluid, Relaxation-Retardation, Viscous Dissipation, Spectral Quasi-Linearization Method.

1. INTRODUCTION

The most promising and inevitable diversified applications of nanofluids today include process industries, heat exchangers, cooling towers, transportation, magneto-optical devices, biomedical-therapeutic treatment and developing the best quality lubricants and oils and many others. Many researchers are giving attention in current years due to huge applications of nanofluids in science and engineering, like oil recovery and drug delivery (Roy et al.[1] and Sobamowo[2]). So, last few years, research on nanofluid flow study is getting more interesting among different researchers like[3–9] etc.

Researchers have challenged and expanded the existing frontiers of scientific knowledge in heat transport and boundary layer fluid flows[10–14]. The Oldroyd-B model is one of the many models that are encountered in the study of non-Newtonian flows. The constitutive model for Oldroyd-B fluids takes into account the impact of both relaxation and retardation times. Some exceptional cases of the Oldroyd-B model include Maxwell and viscous fluid models, Riaz et al.[15]. The Oldroyd-B fluid has uses in heat exchangers or as a coolant. Because of many modern applications, non-Newtonian fluids have been studied extensively as heat and mass transport fluids.[16–18] Bhatnagar et al.[19] studied the Oldroyd-B fluid flow over a linearly deformed surface. Sajid et al.[20] analyzed the stagnation point flow of an Oldroyd-B fluid while neglecting the extra stress tensor components from the momentum expression. Related studies on three dimensional Oldroyd-B fluid can be found in Refs. [21–23].

The Fourier model's weaknesses[24] were addressed in the study by Cattaneo[25] with the introduction of thermal relaxation time. Christov[26] modified Cattaneo's model by replacing the upper-convected time derivative with an ordinary derivative. This is the now well known

*Author to whom correspondence should be addressed.
Email: sabya.mondal.2007@gmail.com
Received: 5 May 2021
Accepted: 15 June 2021

Cattaneo-Christov heat flux model. The Cattaneo-Christov heat flux model with thermal instability was analyzed by Haddad.[27] The impact of the flow of a Cattaneo-Christov heat flux model on the flow of viscoelastic fluid was examined by Han et al.[28] The flow of a magnetohydrodynamic Williamson fluid using the Cattaneo-Christov heat flux model was investigated by Salahuddin et al.[29] The study of chemical reactions is significant due to their extensive industrial and technological applications such as chemical processing equipment, glass making, food preparation, and evaporation from a surface.[30–33]

There are, however, few studies on the three-dimensional rotating flow of an Oldroyd-B nanofluid with relaxation-retardation, viscous dissipation, and nonlinear convection. The main aim of this study is to investigate the role of relaxation-retardation, viscous dissipation, nonlinear thermal radiation, nonlinear convection, and variable chemical reaction on the three-dimensional rotating flow of an Oldroyd-B nanofluid past an exponentially extended surface. The spectral quasi-linearization method is used to find solutions of reduced transport equations. The effects of the physical parameters on the velocity, thermal, and concentration fields were analyzed.

2. FORMULATION OF THE PROBLEM

It is assumed that the surface deforms continuously in x- and y-directions with velocities U_w and V_w, respectively. The momentum equation is modelled by rotation and non-linear convection mechanism. Heat transfer analysis of radiative fluid is explored by implementing famous Buongiorno model and relaxation and retardation viscous dissipation model in the energy equation. In addition, variable chemical reaction model is included in the concentration equation. Such phenomena are invoked to explore their influence in the flow and heat transfer in engineering and industrial applications.

The continuity and momentum equations may be expressed in vector form as:

$$\nabla \cdot V = 0$$

$$(V\cdot\nabla)V + \Omega\times(\Omega\times r) + 2\Omega\times V = -\frac{1}{\rho}\nabla p + \frac{1}{\rho}(\nabla\cdot S) - \frac{\sigma B_0^2}{\rho}\{V + \lambda_1 w(\nabla V)\} + g\left\{\alpha_1(T-T_\infty) + \alpha_2(T-T_\infty)^2\right\} + g\left\{\alpha_3(C-C_\infty) + \alpha_4(C-C_\infty)^2\right\}$$

The term $\Omega\times(\Omega\times r) = -\nabla((\Omega^2 r^2)/2)$ represents the centrifugal acceleration which is being balanced by the pressure gradient $(-\nabla p)$. In the above equation, S is the extra stress tensor for Oldroyd-B fluid and is given by

$$S + \lambda_1\frac{DS}{Dt} = \mu\left(A + \lambda_2\frac{DA_1}{Dt}\right)$$

Where $A_1 = \nabla V + (\nabla V)^T$ is the first-Rivlin Ericksen tensor and (D/Dt) is the upper convected time derivative. For a second rank tensor S and vector $\vec{a}$, we have,

$$\frac{DS}{Dt} = \frac{\partial S}{\partial t} + (V\cdot\nabla)S - LS - SL^T$$

and

$$\frac{D\vec{a}}{Dt} = \frac{\partial\vec{a}}{\partial t} + (V\cdot\nabla)\vec{a} - L\vec{a}$$

Now assigning the operator $(1+\lambda_1(D/Dt))$ and using the above useful information the component forms of the resulting equations after using boundary layer approximations are expressed as follows. Here, we choose the Cartesian coordinates in such a way that x-axis is along the stretching sheet and y-axis perpendicular to sheet. The induced magnetic field and electric field are neglected. The fluid is electrically conducting with an applied magnetic field of strength B_0. Let (u, v, w) be the velocity components along x, y and z directions, respectively (see Fig. 1). The velocity, temperature and concentration fields are governed by the following three-dimensional boundary layer equations.[21–23]

$$\frac{\partial u}{\partial x} + \frac{\partial v}{\partial y} + \frac{\partial w}{\partial z} = 0, \tag{1}$$

$$u\frac{\partial u}{\partial x} + v\frac{\partial u}{\partial y} + w\frac{\partial u}{\partial z} - 2\Omega v + \lambda_1\left[u^2\frac{\partial^2 u}{\partial x^2} + v^2\frac{\partial^2 u}{\partial y^2} + w^2\frac{\partial^2 u}{\partial z^2} + 2uv\frac{\partial^2 u}{\partial x\partial y} + 2vw\frac{\partial^2 u}{\partial y\partial z} + 2uw\frac{\partial^2 u}{\partial x\partial z} - 2\Omega\left(u\frac{\partial v}{\partial x} + v\frac{\partial v}{\partial y} + w\frac{\partial v}{\partial z}\right) + 2\Omega\left(v\frac{\partial u}{\partial x} - u\frac{\partial u}{\partial y}\right)\right] = \nu_f\frac{\partial^2 u}{\partial z^2} + \nu_f\lambda_2\left[u\frac{\partial^3 u}{\partial x\partial z^2} + v\frac{\partial^3 u}{\partial y\partial z^2} + w\frac{\partial^3 u}{\partial z^3} - \frac{\partial u}{\partial x}\frac{\partial^2 u}{\partial z^2} - \frac{\partial u}{\partial y}\frac{\partial^2 v}{\partial z^2} - \frac{\partial u}{\partial z}\frac{\partial^2 w}{\partial z^2}\right] - \frac{\sigma B_0^2}{\rho}\left(u + \lambda_1 w\frac{\partial u}{\partial z}\right)$$

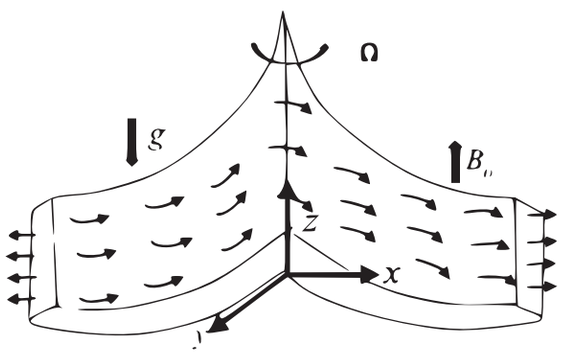

Fig. 1. Schematic diagram.

ARTICLE

$$+g\left\{\alpha_1(T-T_\infty)+\alpha_2(T-T_\infty)^2\right\}$$
$$+g\left\{\alpha_3(C-C_\infty)+\alpha_4(C-C_\infty)^2\right\}, \quad (2)$$

$$u\frac{\partial v}{\partial x}+v\frac{\partial v}{\partial y}+w\frac{\partial v}{\partial z}+2\Omega u+\lambda_1\left[u^2\frac{\partial^2 v}{\partial x^2}+v^2\frac{\partial^2 v}{\partial y^2}+w^2\frac{\partial^2 v}{\partial z^2}+2uv\frac{\partial^2 v}{\partial x\partial y}+2vw\frac{\partial^2 v}{\partial y\partial z}+2uw\frac{\partial^2 v}{\partial x\partial z}-2\Omega\left(u\frac{\partial u}{\partial x}+v\frac{\partial u}{\partial y}+w\frac{\partial u}{\partial z}\right)+2\Omega\left(v\frac{\partial v}{\partial x}-u\frac{\partial v}{\partial y}\right)\right]$$
$$=\upsilon_f\frac{\partial^2 v}{\partial z^2}+\upsilon_f\lambda_2\left[u\frac{\partial^3 v}{\partial x\partial z^2}+v\frac{\partial^3 v}{\partial y\partial z^2}+w\frac{\partial^3 v}{\partial z^3}-\frac{\partial v}{\partial x}\frac{\partial^2 u}{\partial z^2}-\frac{\partial v}{\partial y}\frac{\partial^2 v}{\partial z^2}-\frac{\partial v}{\partial z}\frac{\partial^2 w}{\partial z^2}\right]-\frac{\sigma B_0^2}{\rho}\left(u+\lambda_1 w\frac{\partial u}{\partial z}\right), \quad (3)$$

$$u\frac{\partial T}{\partial x}+v\frac{\partial T}{\partial y}+w\frac{\partial T}{\partial z}=\frac{k_f}{(\rho c_p)_f}\frac{\partial^2 T}{\partial z^2}+\tau\left[D_B\frac{\partial C}{\partial z}\frac{\partial T}{\partial z}+\frac{D_T}{T_\infty}\left(\frac{\partial T}{\partial z}\right)^2\right]+\frac{\lambda_2}{\lambda_1}\left(\frac{\upsilon_f}{c_p}\right)\left[\left(\frac{\partial u}{\partial z}\right)^2+\left(\frac{\partial v}{\partial z}\right)^2\right]-\frac{1}{(\rho c_p)_f}\frac{\partial q_r}{\partial z}, \quad (4)$$

$$u\frac{\partial C}{\partial x}+v\frac{\partial C}{\partial y}+w\frac{\partial C}{\partial z}=D_B\frac{\partial^2 C}{\partial z^2}+\frac{D_T}{T_\infty}\frac{\partial^2 T}{\partial z^2}-K(C-C_\infty) \quad (5)$$

Using the Rosseland approximation, the radiative heat flux is

$$q_r=-\frac{4\sigma^*}{3k^*}\frac{\partial T^4}{\partial z}=-\frac{16\sigma^*}{3k^*}\left(T^3\frac{\partial T}{\partial z}\right) \quad (6)$$

Equation (4) then becomes

$$u\frac{\partial T}{\partial x}+v\frac{\partial T}{\partial y}+w\frac{\partial T}{\partial z}=\frac{k_f}{(\rho c_p)_f}\frac{\partial^2 T}{\partial z^2}+\tau\left[D_B\frac{\partial C}{\partial z}\frac{\partial T}{\partial z}+\frac{D_T}{T_\infty}\left(\frac{\partial T}{\partial z}\right)^2\right]+\frac{\lambda_2}{\lambda_1}\left(\frac{\upsilon_f}{c_p}\right)\left[\left(\frac{\partial u}{\partial z}\right)^2+\left(\frac{\partial v}{\partial z}\right)^2\right]+\frac{16\sigma^*}{3k^*(\rho c_p)_f}\frac{\partial}{\partial z}\left(T^3\frac{\partial T}{\partial z}\right). \quad (7)$$

The associated boundary conditions are

$$u=U_w,\quad v=V_w,\quad w=0,$$
$$-k_f\left(\frac{\partial T}{\partial z}\right)=h_1(T_w-T),$$
$$-D_B\left(\frac{\partial C}{\partial z}\right)=h_2(C_w-C),\quad \text{at}\quad z=0,$$
$$u\to 0,\quad v\to 0,\quad T\to T_\infty,$$
$$C\to C_\infty,\quad \text{as}\quad z\to\infty \quad (8)$$

Here, $U_w=U_0\exp((x+y)/L)$ and $V_w=V_0\exp((x+y)/L)$ are stretching velocities with U_0 and V_0 as reference velocities, $T_w=T_\infty+T_0\exp[(A(x+y))/2L]$ and $C_w=C_\infty+C_0\exp[(B(x+y))/2L]$ are surface temperature and concentration respectively, $K=K_0\exp((x+y)/L)$ (K_0 as constant) is the variable chemical reaction rate.

The appropriate transformations used are

$$\eta=\sqrt{\frac{U_0}{2\upsilon_f L}}\exp\left[\frac{x+y}{2L}\right]z,$$
$$u=U_0\exp\left[\frac{x+y}{L}\right]F'(\eta),$$
$$v=U_0\exp\left[\frac{x+y}{L}\right]G'(\eta),$$
$$w=-\sqrt{\frac{\upsilon_f U_0}{2L}}\exp\left[\frac{x+y}{2L}\right][F(\eta)+\eta F'(\eta)+G(\eta)+\eta G'(\eta)],\quad \theta(\eta)=\frac{T-T_\infty}{T_w-T_\infty},$$
$$\phi(\eta)=\frac{C-C_\infty}{C_w-C_\infty}, \quad (9)$$

From (9), $T=T_\infty[1+(\theta_w-1)\theta]$, where $\theta_w=(T_w/T_\infty)$ is the temperature parameter.

Using Eq. (9), Eqs. (2)–(5) become

$$F'''+(F+G)F''-2(F'+G')F'+4\lambda G'+\Gamma_1[(3F''+\eta F''')((F+G)(F'+G')+\eta(F'^2+G'^2)+2\eta F'G')-F'G'(4F'+5\eta F''+\eta^2F''')-(F'^2+G'^2)(2F'+2.5\eta F''+0.5\eta^2F''')-2F'''((F+G)+\eta(F'+G'))^2+\lambda(2(F'^2+G'^2)-(F+G)G''+\eta(F'-G')F'')]+\Gamma_2[2(F'+G')F'''+(\eta(F'+G')+0.5(F+G))\times F^{iv}-(F'''+G''')F'-(1.5(F''+G'')F''+\eta(F'''+G''')F'')]-2MF'+M\Gamma_1F''[(F+G)+\eta(F'+G')]+2\lambda_T(1+\beta_1\theta)\theta+2\lambda_T N(1+\beta_2\phi)\phi=0, \quad (10)$$

$$G'''+(F+G)G''-2(F'+G')G'-4\lambda F'+\Gamma_1[(3G''+\eta G''')((F+G)(F'+G')+\eta(F'^2+G'^2)+2\eta F'G')-F'G'(4G'+5\eta G''+\eta^2G''')-(F'^2+G'^2)(2G'+2.5\eta G''+0.5\eta^2G''')$$

$$-2G'''((F+G)+\eta(F'+G'))^2$$
$$+\lambda(2(F'^2+G'^2)-(F+G)F''+\eta(F'-G')G'')]$$
$$+\Gamma_2[2(F'+G')G'''+(\eta(F'+G')+0.5(F+G))G^{iv}$$
$$-(F'''+G''')G'-(1.5(F''+G'')G''$$
$$+\eta(F'''+G''')G'')]-2MG'$$
$$+M\Gamma_1G''[(F+G)+\eta(F'+G')]=0, \quad (11)$$

$$[1+Rd(1+(\theta_w-1)\theta)^3]\theta''$$
$$+3(\theta_w-1)[1+(\theta_w-1)\theta]^2\theta'^2$$
$$+Pr[(F+G)\theta'+N_b\theta'\phi'+N_t(\theta')^2$$
$$+E_{cm}(F''^2+G''^2)]=0 \quad (12)$$

$$\phi''+Sc(F+G)\phi'+\left(\frac{Nt}{Nb}\right)\theta''-Sc\gamma\phi=0, \quad (13)$$

with the resulting boundary conditions

$$F(0)=0,\quad G(0)=0,\quad F'(0)=1,\quad G'(0)=\beta,$$
$$\theta'(0)=-B_1[1-\theta(0)],\quad \phi'(0)=-B_2[1-\phi(0)]$$
$$\text{at}\quad \eta\to 0$$
$$F'\to 0,\quad G'\to 0,\quad F''\to 0,\quad G''\to 0,$$
$$\theta\to 0,\quad \phi\to 0,\quad \text{as}\quad \eta\to\infty \quad (14)$$

where

$$\Gamma_1=\frac{\lambda_1U_0\exp((x+y)/L)}{L},\quad \Gamma_2=\frac{\lambda_2U_0\exp((x+y)/L)}{L},$$
$$M=\frac{2L\sigma B_0^2}{\rho U_0\exp((x+y)/L)},\quad \lambda=\frac{\Omega L}{U_w^2},$$
$$N=\frac{Gr^*}{Gr}=\frac{\alpha_3(C_w-C_\infty)}{\alpha_1(T_w-T_\infty)},$$
$$Gr=\frac{g\alpha_1(T_w-T_\infty)L^3}{\upsilon^2},\quad Gr^*=\frac{g\alpha_3(C_w-C_\infty)L^3}{\upsilon^2},$$
$$\beta_1=\frac{\alpha_2(T_w-T_\infty)}{\alpha_1},\quad \beta_2=\frac{\alpha_4(C_w-C_\infty)}{\alpha_3},$$
$$\Pr=\frac{\upsilon_f}{\alpha_f},\quad \gamma=\frac{2KL}{U_w},\quad \beta=\frac{V_0}{U_0},\quad Sc=\frac{\upsilon_f}{D_B},\quad \lambda_T=\frac{Gr}{Re_x^2},$$

Table I. Values of the skin friction coefficients, Nusselt and Sherwood number with β when $\lambda=0.1, \lambda_T=0, \gamma=1, \Gamma_1=0.1, \Gamma_2=0.1, N=1, M=0.5, \beta_1=0.1, \beta2=0.1, Rd=2, Pr=5, Nb=0.5, Nt=0.3, Ecm=0.1, \theta_w=2, Sc=1, B_1=0.5$ and $B_2=0.5$.

β	$F''(0)$	$G''(0)$	$-\theta'(0)$	$-\phi'(0)$
0	1.741834	0.127845	0.177131	0.058962
0.2	1.855033	0.496200	0.207644	0.050082
0.4	1.968169	0.919780	0.236839	0.04135
0.6	2.081585	1.397291	0.265105	0.032729
0.8	2.195540	1.928011	0.292703	0.024182
1.0	2.310237	2.511605	0.319822	0.015675

Table II. Residual error for the functions when $\lambda=0.2, \lambda_T=0.1, \gamma=1, \Gamma_1=0.2, \Gamma_2=0.2, N=1, M=0.5, \beta=0.5, \beta_1=0.1, \beta2=0.1, Rd=2, Pr=1, Nb=0.3, Nt=0.5, Ecm=0.1, \theta_w=2, Sc=1, B_1=0.5$ and $B_2=0.5$.

Iter	$\| Res(F) \|_\infty$	$\| Res(G) \|_\infty$	$\| Res(\theta) \|_\infty$	$\| Res(\phi) \|_\infty$
1	4.81e−07	5.21e−07	2.27e−08	2.73e−09
2	3.42e−08	3.81e−08	4.22e−09	3.30e−10
3	3.24e−09	6.06e−09	7.21e−10	3.74e−11
4	5.57e−10	2.82e−09	3.29e−10	1.11e−11
5	2.64e−10	3.33e−10	3.00e−12	1.05e−12
6	5.99e−10	1.07e−10	1.77e−12	1.48e−13
7	1.90e−10	9.97e−11	1.02e−12	1.39e−12
8	8.01e−11	4.12e−11	6.60e−13	3.05e−13
9	5.73e−11	1.96e−11	6.92e−13	3.66e−13
10	7.71e−11	2.95e−11	7.21e−13	2.90e−13

$$Re_x=\frac{U_wL}{\upsilon_f},\quad Rd=\frac{16\sigma^*T_\infty^3}{3kk^*},\quad Nb=\frac{\tau D_B(C_w-C_\infty)}{\upsilon_f},$$
$$Nt=\frac{\tau(T_w-T_\infty)D_T}{T_\infty\upsilon_f},\quad B_1=\frac{h_1}{k_f\sqrt{\frac{U_w}{2\upsilon_fL}}},$$
$$B_2=\frac{h_2}{D_B\sqrt{\frac{U_w}{2\upsilon_fL}}},\quad E_{cm}=\frac{\lambda_2U_w^2}{\lambda_1c_p(T_w-T_\infty)}.$$

The parameters of interest in dimensionless form are:
Axial skin friction coefficient, $((Re/2))^{(1/2)}C_{fx}=F''(0)$
Transverse skin friction coefficient, $((Re/2))^{(1/2)}C_{fy}=G''(0)$
Local Nusselt number, $((Re/2))^{-(1/2)}Nu_x=-[1+Rd\{(\theta_w-1)\theta(0)+1\}^3]\theta'(0)$
Local Sherwood number $((Re/2))^{-(1/2)}Sh_x=-\phi'(0)$
where $Re=(U_wL)/\upsilon_f$ is the local Reynolds number.

3. METHOD OF SOLUTION

We solve the highly coupled equations with the associating boundary conditions using the spectral quasi-linearization

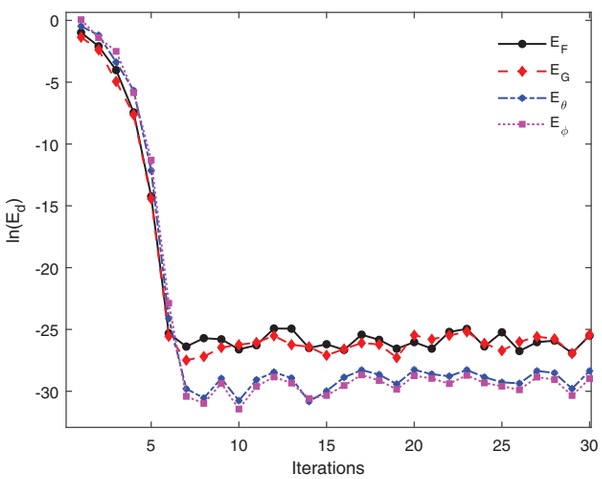

Fig. 2. Convergence graphs for the functions.

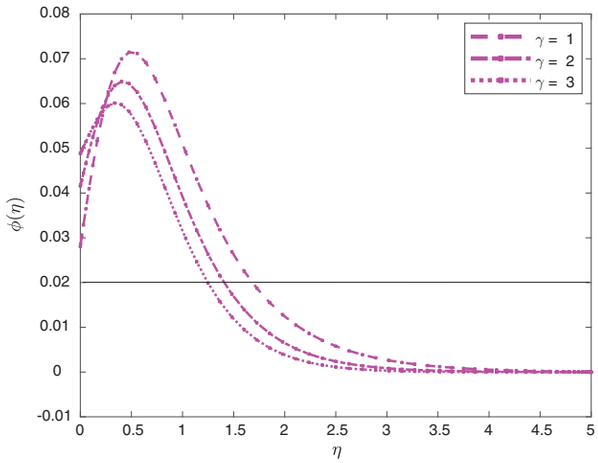

Fig. 3. Concentration profile with different values of chemical reaction parameter.

method. The quasi-linearization technique assumes a Taylor series expansion with the assumption that there exists minimal error when taking the difference between previous and current iteration. The quasi-linearisation follows the format given by Bellman and Kalaba.[34] The equations are linearized and then solved as a coupled equation using the spectral collocation method. We transform the infinite domain of the boundary condition to Gauss-Lobatto pints using a linear transformation. Starting with suitable initial values, the equations are solved iteratively to obtain accurate and convergent solutions which was proposed by Motsa.[35] A detailed description of the method may be found in some articles like Motsa et al.[36] and Oyelakin et al.[37]

3.1. Method Description

The system of nonlinear ordinary differential equations given in Eqs. (10)–(13), are written as a sum of its linear and nonlinear components and the nonlinear components linearised using one term Taylor series for multiple variables to give the following:

$$a_{0,r}F^{iv}_{r+1} + a_{1,r}F^{'''}_{r+1} + a_{2,r}F^{''}_{r+1} + a_{3,r}F^{'}_{r+1} + a_{4,r}F_{r+1} + a_{5,r}G^{'''}_{r+1} + a_{6,r}G^{''}_{r+1} + a_{7,r}G^{'}_{r+1} + a_{8,r}G_{r+1} + a_{9,r}\theta_{r+1} + a_{10,r}\phi_{r+1} = R_{1,r} \quad (15)$$

$$b_{0,r}G^{iv}_{r+1} + b_{1,r}G^{'''}_{r+1} + b_{2,r}G^{''}_{r+1} + b_{3,r}G^{'}_{r+1} + b_{4,r}G_{r+1} + b_{5,r}F^{'''}_{r+1} + b_{6,r}F^{''}_{r+1} + b_{7,r}F^{'}_{r+1} + b_{8,r}F_{r+1} = R_{2,r} \quad (16)$$

$$c_{0,r}\theta^{''}_{r+1} + c_{1,r}\theta^{'}_{r+1} + c_{2,r}\theta_{r+1} + c_{3,r}F^{''}_{r+1} + c_{4,r}F_{r+1} + c_{5,r}G^{''}_{r+1} + c_{6,r}G_{r+1} + c_{7,r}\phi^{'}_{r+1} = R_{3,r} \quad (17)$$

$$d_{0,r}\phi^{''}_{r+1} + d_{1,r}\phi^{'}_{r+1} + d_{2,r}\phi_{r+1} + d_{3,r}f_{r+1} + d_{4,r}g_{r+1} + d_{5,r}\theta^{''}_{r+1} = R_{4,r} \quad (18)$$

where the variable constants $a_{i,r}$, $b_{i,r}$, $c_{i,r}$, $d_{i,r}$ and $R_{i,r}(i = 1, 2, 3, \ldots)$ are known from previous calculations. The boundary conditions are given as

$$F_{r+1}(0) = 0, \quad G_{r+1}(0) = 0, \quad F'_{r+1}(0) = 1,$$
$$G'_{r+1}(0) = \beta, \quad \theta'_{r+1}(0) = -B_1\left[1 - \theta_r(0)\right],$$
$$\phi'_{r+1}(0) = -B_2\left[1 - \phi_r(0)\right]$$
$$F'_{r+1}(\infty) \to 0, \quad G'_{r+1}(\infty) \to 0, \quad F''_{r+1}(\infty) \to 0,$$
$$G''_{r+1}(\infty) \to 0, \quad \theta_{r+1}(\infty) \to 0, \quad \phi_{r+1}(\infty) \to 0 \quad (19)$$

Equations (16)–(18) form the iterative scheme for the spectral quasi-linearisation method and it is then solved using the Chebyshev spectral collocation method. Starting with suitable initial approximations, the iteration schemes (16)–(18) are then solved iteratively for F_{r+1}, G_{r+1}, θ_{r+1}, and ϕ_{r+1} when $r = 0, 1, 2, \ldots$

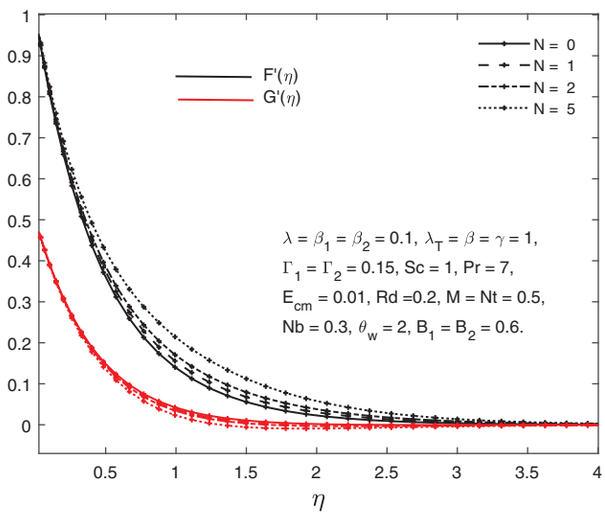

Fig. 4. Buoyancy forces ratio.

4. RESULTS AND DISCUSSION

The out comes of the results are shown through some figures and tables. All the parameters are chooses here based on the previously published papers. Table I endorses the influence of β on axial skin friction coefficient $F''(0)$ and transverse skin friction coefficient $G''(0)$, Nusselt number $-\theta'(0)$ and Sherwood number $-\phi'(0)$ when $\lambda = 0.1, \lambda_T = 0, \gamma = 1, \Gamma_1 = 0.1, \Gamma_2 = 0.1, N = 1, M = 0.5, \beta_1 = 0.1, \beta 2 = 0.1, Rd = 2, Pr = 5, Nb = 0.5, Nt = 0.3, Ecm = 0.1, \theta_w = 2, Sc = 1, B_1 = 0.5$ and $B_2 = 0.5$. It is clearly understood from the numerical table that amplifying β yields the augmentation of $F''(0)$, $G''(0)$ and $-\theta'(0)$ while it shows opposite effect (diminution) for $-\phi'(0)$.

To demonstrate the accuracy of the spectral quasi-linearization method, we use the residual error norm at infinity. Table II shows the convergence of the method to accurate results by the 10th iteration. We observe that the error is relatively small. It is of order (10^{-11}). The convergence of the method is further illustrated in Figure 2,

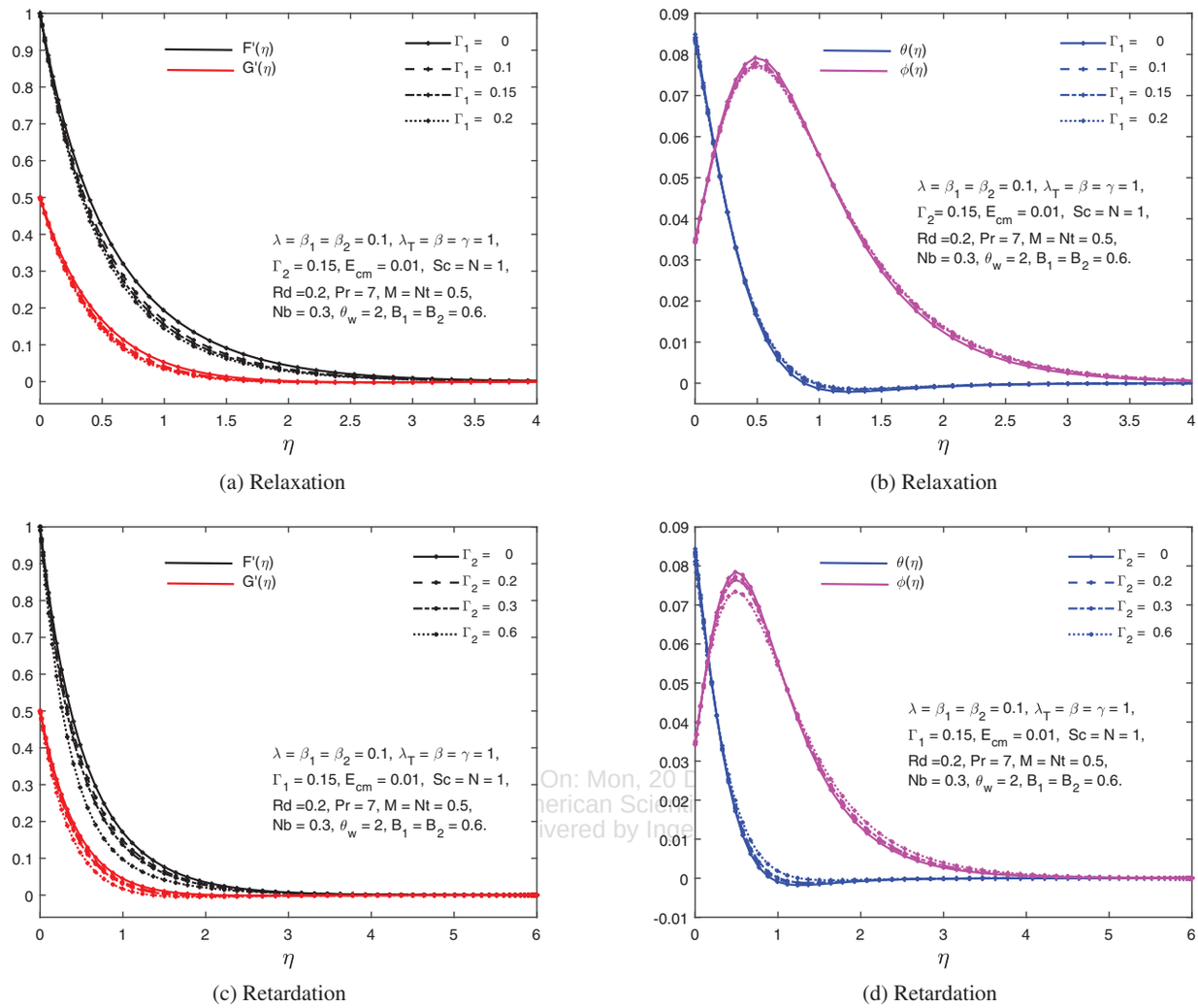

Fig. 5. Effect of relaxation and retardation parameters on the velocity, temperature, and concentration profiles.

which shows the solution error norms as a function of the number of iterations. The norm is a measure of the difference between the current and previous solution vector of each function. This error is evaluated using the error norm at infinity. We note that even from the 5th iteration, the method gives a good convergence rate. Figure 3 displays the concentration profile for different values of chemical reaction parameter. It is seen from this figure that concentration profiles increase with the increase in values of chemical reaction parameters close to the wall and an opposite trend is observed after that i.e., way from the wall. Similar results can be found in Ref. [38].

Figure 4 shows the impact of the buoyancy ratio parameter on the velocity profiles. As the parameter increases, the velocity profile $F'(\eta)$ increases, while the velocity profile $G'(\eta)$ decreases. The buoyancy force creates an upward force, which produces a net force. This is due to the difference between the pressure at the depth of the fluid and the top. This net force enhances the fluid motion, as shown in the velocity profile $F'(\eta)$. The effect of the parameter on velocity profile $G'(\eta)$ is a negligible decrease.

Figure 5 shows the impact of relaxation and retardation parameters on the velocity, temperature, and concentration profiles. An increase in the relaxation and retardation parameters decreases both the $F'(\eta)$ and $G'(\eta)$ velocity profiles. This implies an opposing flow due to viscoelastic properties. However, the parameters give an insignificant increase in both temperature and concentration profiles. Figure 5(a) addresses the behavior of $F'(\eta)$ and $G'(\eta)$ for varied estimations of Γ_1, $(\Gamma_1 = 0, 0.1, 0.15, 0.2)$. It is conveying to the point that $F'(\eta)$ and $G'(\eta)$ diminish for larger Γ_1. In fact, for higher Γ_1, the relaxation time of the Oldroyd-B nanofluid rises. This implies that the viscous force enhances and optimally resists the motion of the Oldroyd-B nanofluid. It is expected that Oldroyd-B nanofluids with larger relaxation time behave as elastically solid-like materials. As a consequence, this reduces the

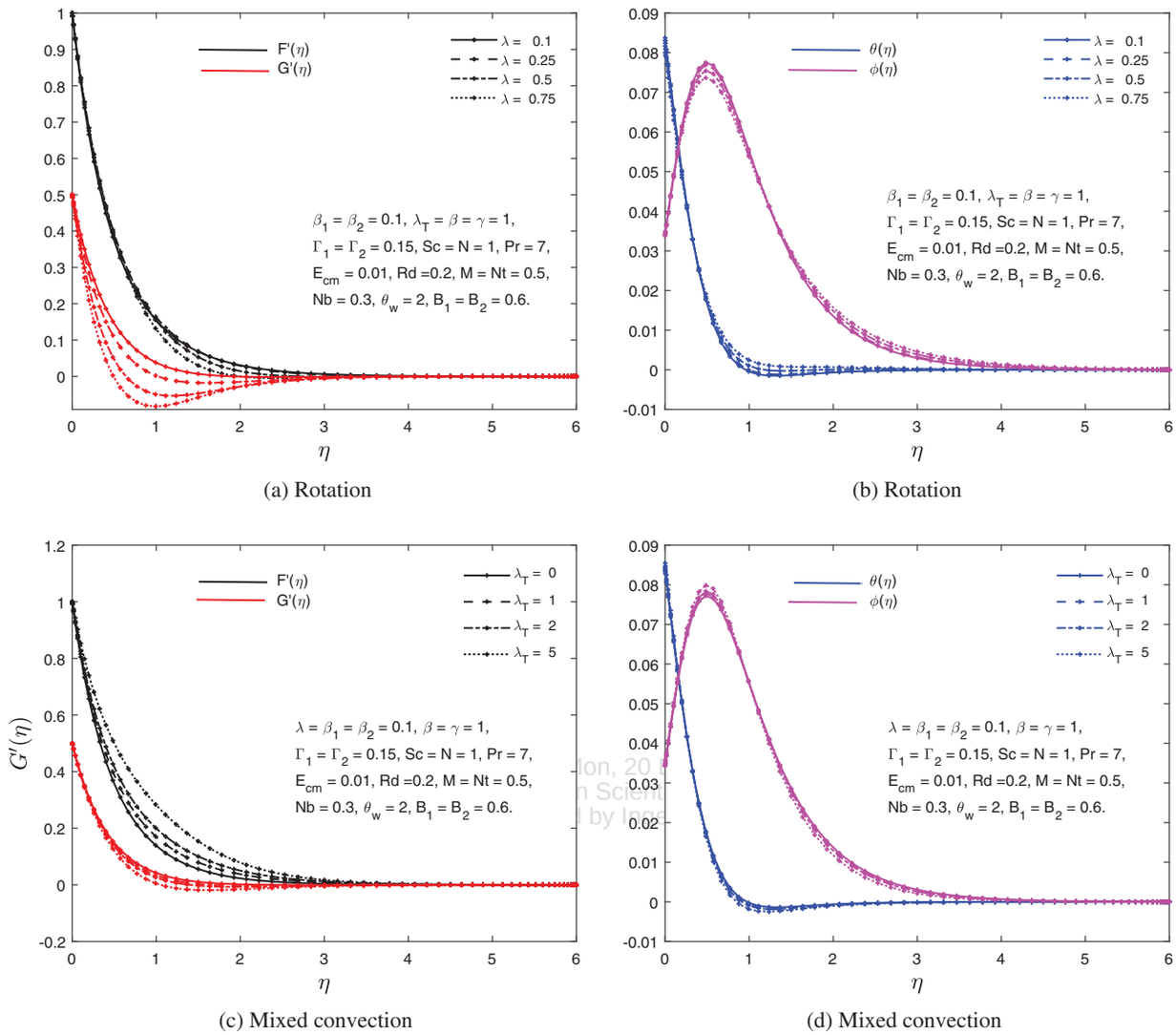

Fig. 6. Effect of rotation and mixed convection parameters on the velocity, temperature, and concentration profiles.

motion of the Oldroyd-B nanofluid along the flow directions. For small relaxation parameter $\Gamma_1 = 0.1$, there is a monotonic decrease in $F'(\eta)$ and $G'(\eta)$ in the boundary layer region. When Γ_1 rises gradually, the profiles of $F'(\eta)$ and $G'(\eta)$ get shifted towards the wall. The flows along axial and transverse directions are resisted by viscoelastic effect. This characteristic is different from that of elastic parameter of second grade fluid. Figure 5(b) is drawn to convey the behavior of temperature $\theta(\eta)$ and concentration $\phi(\eta)$ for different estimations of Γ_1. It is envisaged that the resistance to the fluid motion due to relaxation time uplifts $\theta(\eta)$ and $\phi(\eta)$ and the related boundary layers thickness. Figure 5(c) demonstrates the nature of $F'(\eta)$ and $G'(\eta)$ in relation to different values of Γ_2, $(\Gamma_2 = 0, 0.2, 0.3, 0.6)$. Figure 5(d) shows that the effect of Γ_2 on $\theta(\eta)$ and $\phi(\eta)$ is qualitatively opposite to that of Γ_1.

The impact of rotation and mixed convection parameters on the velocity, temperature, and concentration profiles are shown in Figure 6. The rotation parameter has a significant impact on the $G'(\eta)$ velocity profiles, as noted in Figure 6(a). The profile significantly reduces as the parameter increases. For both $F'(\eta)$ and $G'(\eta)$ profiles, the velocity is noted to decrease. An increase in the rotation parameter causes a strain and decay on the velocity profiles. Again, we note in Figure 6(b) an insignificant increase and decrease in the temperature and concentration profiles, respectively. Figures 6(c) and (d) show that while $F'(\eta)$ velocity profile increases, the $G'(\eta)$ velocity profile decreases as the parameter is increased. Nevertheless, the parameter has a minor effect on both temperature and concentration profiles.

The magnetic field parameter generates the resistive Lorentz force in fluids, which tends to slow fluid motion.

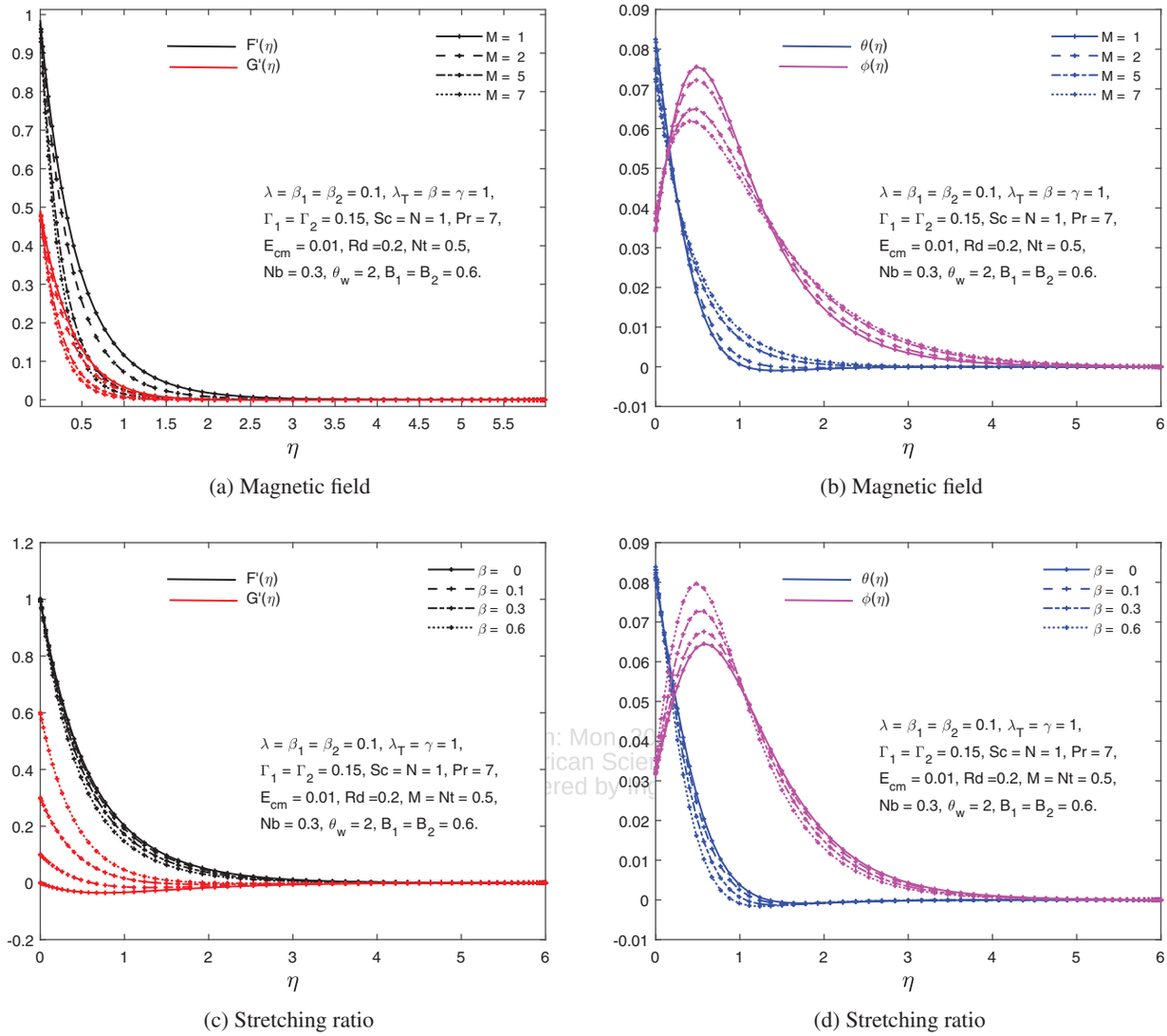

Fig. 7. Effect of magnetic field and stretching ratio parameters on the velocity, temperature, and concentration profiles.

The effect of the parameter is shown in Figure 7(a). Figure 7(b) shows the effect of the parameter on the temperature and concentration profiles. As expected, an increasing magnetic field parameter enhances the profiles. Figures 7(c) and (d) show the impact of the stretching ratio parameter on the velocity, temperature and concentration profiles. Here, we note the parameter's impact is greater in the $G'(\eta)$ velocity profile than the $F'(\eta)$ velocity profile. We also note that the velocity profile $G'(\eta)$ is increasing while the velocity profile of $F'(\eta)$ is decreasing. An increase in the parameter is noted to decrease both temperature and concentration profiles. This is because of the increased entrainment process, which results from an enhancement in the movement of a reduced fluid temperature and particle concentration.

Thermal and solutal heat flux parameters describe convective conditions on temperature and concentration boundaries, respectively. An increase in the thermal heat flux parameter is noted to increase temperature and concentration profiles. This implies a dominant convective heat effect on the boundaries and, as such, an increasing profile. This may be viewed in Figure 8(a). In Figure 8(b), we note that the parameter has a more pronounced effect on the concentration profiles compared to the temperature profiles. This effect shows an enhanced concentration profile as the solutal heat flux parameter is increased. The impact of an increasing modified Eckert number on the temperature and concentration profiles is noted in Figure 8(c). The parameter is noted to have a significant effect on the flow very close to the surface. Far from the surface, the parameter has a

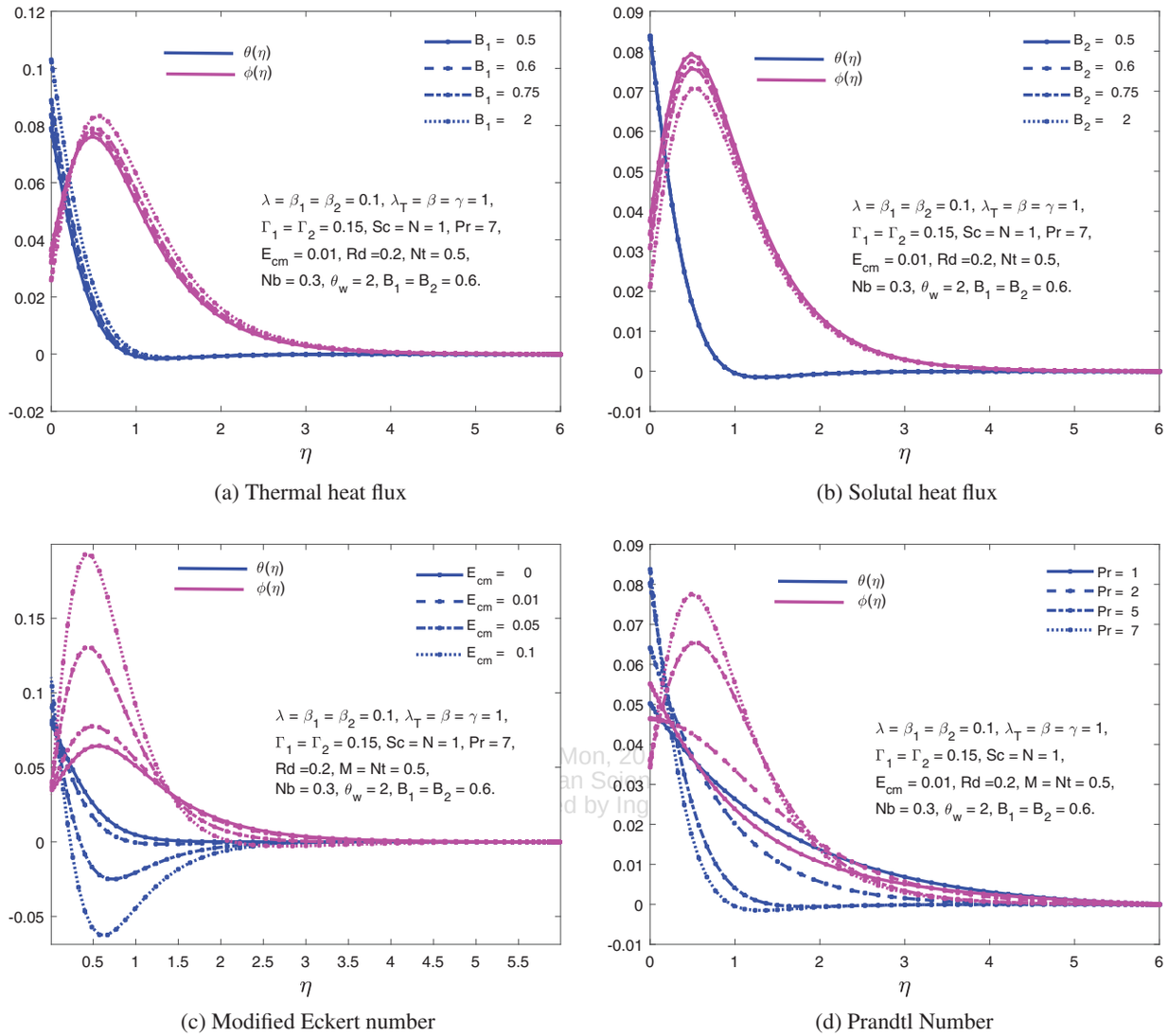

(a) Thermal heat flux

(b) Solutal heat flux

(c) Modified Eckert number

(d) Prandtl Number

Fig. 8. Effect of some parameters on the temperature and concentration profiles.

negligible impact. The parameter increases the concentration profiles while it reduces the temperature profiles. The modified Eckert number is a ratio of velocity to heat capacity; and retardation to relaxation times. An increase in concentration profiles indicates dominant retardation and velocity, while a decrease in the temperature profile indicates a dominant relaxation time and heat capacity. In Figure 8(d), we characterize the impact of the Prandtl number on the temperature and concentration profiles. The Prandtl number is a ratio of viscous to diffusive forces. A larger Prandtl number is an indication that the viscosity forces dominate. This is known to reduce fluid motion, and as such, there is a cooling fluid process.

Figure 9 shows the impact of thermal radiation, surface temperature, and nanoparticle parameters on the temperature and concentration profiles. Figure 9(a) shows that the thermal radiation parameter enhances the temperature profiles while reducing the concentration profiles. Figure 9(b) shows a negligible increase in the temperature profile and a significant decrease in the concentration profiles as the surface temperature parameter increases. In Figures 9(c) and (d), the nanoparticle parameters are noted to have a significant impact on the concentration profiles, while we note the negligible impact on temperature profiles. The particle Brownian motion parameter increases the concentration profile as expected. This parameter allows for the nanoparticles' free movement in the flow; hence an increase is expected. Increasing the thermophoresis parameter, on the other hand, leads to a decreased concentration profile.

A significant decrease in concentration profiles may be viewed in Figure 10(a). This decrease is a result of an increasing chemical reaction. This implies a reduced

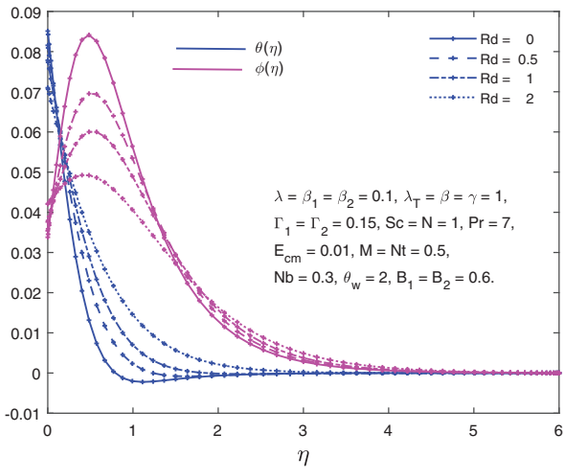

(a) Thermal radiation

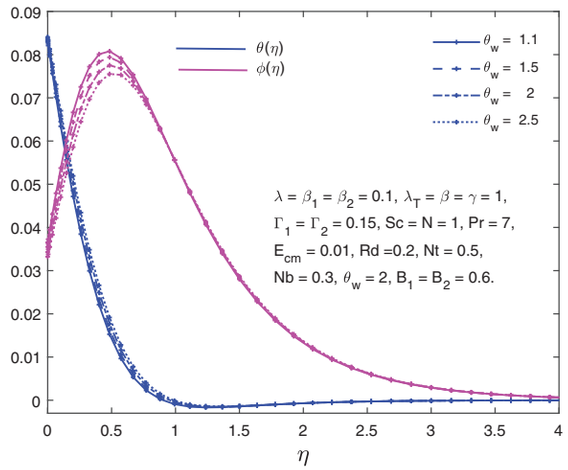

(b) Surface temperature

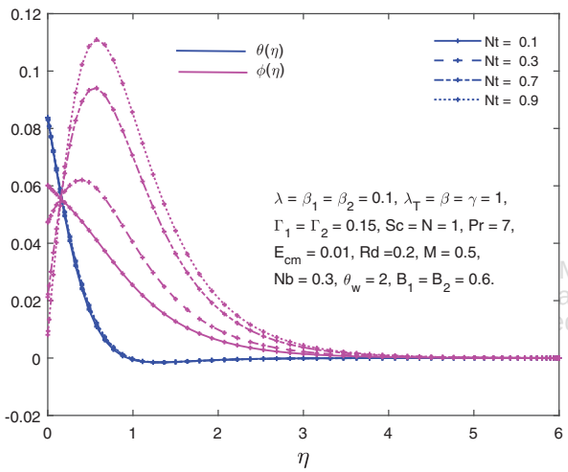

(c) Thermophoresis

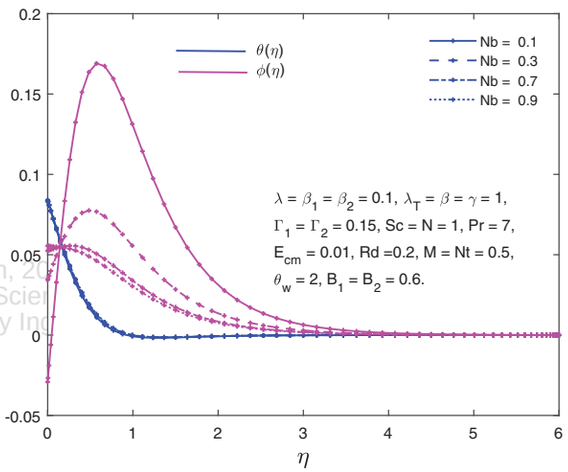

(d) Brownian motion

Fig. 9. Effect of some parameters on the temperature and concentration profiles.

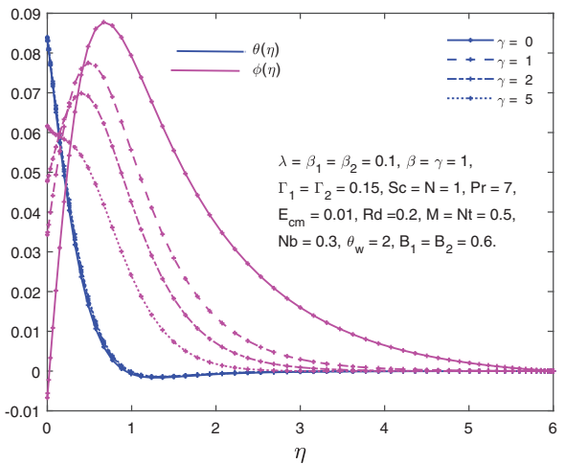

(a) Chemical reaction

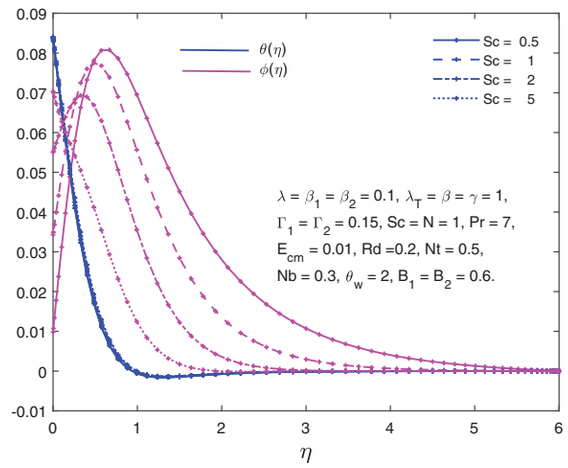

(b) Schmidt number

Fig. 10. Effect of chemical reaction and Schmidt number on the temperature and concentration profiles.

ARTICLE

chemical species interaction in the nanoparticle volume fraction concentration. Again, increasing the Schmidt number is also noted to reduce the concentration profiles significantly (in Fig. 10(b)). We note a negligible impact of both chemical reaction and Schmidt number on the temperature profiles.

5. CONCLUSION

In this study, three dimensional rotating flow of an Oldroyd-B nanofluid with relaxation-retardation viscous dissipation, nonlinear thermal radiation, nonlinear convection and variable chemical reaction over an exponentially extended surface has been investigated. Heat transfer was studied using the Cattaneo-Christov model. We make, among other findings, the following observations:

- The velocity distributions gets diminution due to varied relaxation time opposes the flow while for retardation time favors the momentum transport has opposite nature observed.
- $F'(\eta)$ and $G'(\eta)$ declined due to incremented λ while those belittle with augmented M.
- $\theta(\eta)$ and $\phi(\eta)$ profiles intensify due to strengthening of Γ_1 while those show decaying trend due to the rise in Γ_2.
- Augmented Sc led to the reduction in $\phi(\eta)$.
- Rise in modified Eckert number controls the heat transfer rate from the extended surface which is a new outcome compared to the previously results.

NOMENCLATURE

$u =$ Velocity along x-axis
$v =$ Velocity along y-axis
$w =$ Velocity along z-axis
$T =$ Temperature of the fluid
$T_w =$ Constant temperature at wall
$T_\infty =$ Ambient temperature
$T_f =$ Temperature of the fluid heating on the surface of the stretching sheet
$D_T =$ Thermophoresis diffusion coefficient
$T =$ Temperature of the nanofluid
$C_p =$ Specific heat at constant pressure
$C =$ Concentration of the fluid
$C_\infty =$ Ambient concentration
$C_f =$ Concentration of the fluid on the surface of the stretching sheet
$D_T =$ Thermophoresis diffusion coefficient
$D_B =$ Brownian diffusion coefficient
$C_p =$ Specific heat at constant pressure
$B_0 =$ Magnetic field of strength
$\lambda_1 =$ Fluid relaxation time
$\lambda_2 =$ Fluid retardation time
$\sigma^* =$ Stefan Boltzmann constant
$k^* =$ Mean absorption coefficient
$\rho =$ Density of the fluid
$\Omega =$ $[0, 0, \Omega]$, Angular velocity vector
$g =$ Gravitational acceleration
$\beta_T =$ Volumetric coefficient of thermal expansions
$\beta_C =$ Volumetric coefficient of solutal expansions
$\upsilon_f =$ Kinematic viscosity of the fluid
$\rho_f =$ Density of base fluid
$k_f =$ The thermal conductivity
$\alpha_1 =$ Linear thermal expansions coefficients
$\alpha_2 =$ Nonlinear thermal expansions coefficients
$\alpha_3 =$ Linear concentration expansion coefficients
$\alpha_4 =$ Nonlinear concentration expansion coefficients
$h_1 =$ Convective heat transfer coefficients
$h_2 =$ Convective mass-transfer coefficients
$\Gamma_1 =$ Deborah numbers (in terms of relaxation times)
$\Gamma_2 =$ Deborah numbers (in terms of retardation times)
$\lambda =$ Rotational parameter
$N =$ Ratio of solutal and thermal buoyancy forces
$Gr =$ Thermal Grashof number
$Gr^* =$ Solutal Grashof number
$\beta_1 =$ Non-linear convection parameter due to temperature
$\beta_2 =$ Non-linear convection parameter due to concentration
$Pr =$ Prandtl number
$\gamma =$ Chemical reaction parameter
$\beta =$ Ratio of stretching rates
$Sc =$ Schmidt number
$\lambda_T =$ Mixed convection parameter
$Re_x =$ Reynolds number
$B_1 =$ Deborah numbers (in terms of relaxation time of the heat fluxes)
$B_2 =$ Deborah numbers (in terms of relaxation time of the mass fluxes)
$E_{cm} =$ Modified Eckert number
$C_{fx} =$ Axial skin friction coefficient
$C_{fy} =$ Transverse skin friction coefficient
$Sh_x =$ Sherwood number
$Nu_x =$ Local Nusselt number

Conflict of Interest

The authors declare that they have no conflict of interest.

Acknowledgment: The authors appreciate the support offered by the Amity University Kolkata-700135, West Bengal, India.

References and Notes

1. N. C. Roy, M. A. Hossain, and I. Pop, *J. Appl. Comput. Mech.* 7 19 **(2021)**.
2. G. Sobamowo, *Reports in Mechanical Engineering* 1, 110 **(2020)**.
3. R. V. Lakshmi, G. Sarojamma, and A. J. Chamkha, *Journal of Nanofluids* 9, 133 **(2020)**.
4. N. A. Ahamad, M. V. Krishna, and A. J. Chamkha, *Journal of Nanofluids* 9, 177 **(2020)**.
5. A. J. Chamkha, R. Yassen, M. A. Ismael, A. M. Rashad, T. Salah, and H. A. Nabwey, *Journal of Nanofluids* 9, 1 **(2020)**.

6. R. Devi, V. Poply, and Manimala, *Heat Transfer-Asian Research* 49, 3702 **(2020)**.
7. M. K. Nayak, S. Shaw, and A. J. Chamkha, *Journal of Nanofluids* 7, 646 **(2018)**.
8. M. K. Nayak, S. Shaw, O. D. Makinde, and A. J. Chamkha, *Journal of Nanofluids* 7, 657 **(2018)**.
9. S. Mondal, S. K. Nandy, and P. Sibanda, *Journal of Nanofluids* 7, 995 **(2018)**.
10. A. J. Chamkha, A. S. Dogonchi, and D. D. Ganji, *AIP Advances* 9, 025103 **(2019)**.
11. F. Selimefendigi, H. F. A–ztop, and A. J. Chamkha, *Int. J. Num. Meth. Heat Fluid Flow* 30, 1755 **(2019)**.
12. A. I. Alsabery, M. A. Ismael, A. J. Chamkha, and I. Hashim, *Int. J. Heat Mass Transf.* 119, 939 **(2018)**.
13. S. Parvin, R. Nasrin, M. A. Alim, N. F. Hossain and A. J. Chamkha, *Int. J. Heat Mass Transf.* 55, 5268 **(2012)**.
14. M. Ghalambaz, S. A. Mehryan, I. Zahmatkesh, and A. J. Chamkha, *Int. J. Therm. Sci.* 157, 106503 **(2020)**.
15. M. B. Riaz, M. A. Imran, and K. Shabbir, *Alexandria Engineering Journal* 55, 3267 **(2016)**.
16. R. Comminal, J. H. Hattel, M. A. Alves, and J. Spangenberg, *J. Non-Newton. Fluid Mech.* 237, 1 **(2016)**.
17. C. Fetecau and C. Fetecau, *International Journal of Engineering Science* 43, 340 **(2005)**.
18. K. R. Rajagopal and A. R. Srinivasa, *J. Non-Newton. Fluid Mech.* 88, 207 **(2000)**.
19. R. K. Bhatnagar, G. Gupta, and K. R. Rajagopal, *Int. J. Non-Linear Mech.* 30, 391 **(1995)**.
20. M. Sajid, Z. Abbas, T. Javed, and N. Ali, *Can. J. Phys.* 88, 635 **(2010)**.
21. A. Aziz, T. Muhammad, A. Alsaedi, and T. Hayat, *J. Brazilian Soci. Mech. Sci. Eng.* 41, 236 **(2019)**.
22. A. Farooq, R. Ali, and A. C. Benim, *Physica A* 503, 345 **(2018)**.
23. M. Mustafa, T. Hayat, and A. Alsaedi, *International Journal of Numerical Methods for Heat and Fluid Flow* 27, 2207 **(2017)**.
24. J. Fourier, *Analytical theory of heat*, (Cambridge Library Collection-Mathematics) (A. Freeman, Trans.). Cambridge University Press, Cambridge, **2009** DOI: 10.1017/CBO9780511693205.
25. C. Cattaneo, ed., *Sulla Conduzione Del Calore.* In: Pignedoli A. (eds) Some Aspects of Diffusion Theory. C.I.M.E. Summer Schools, Vol. 42, Springer, Berlin, Heidelberg, **2011**.
26. C. I. Christov, *Mech. Research Commun.* 36, 481 **(2009)**.
27. S. A. M. Haddad, *Int. J. Heat Mass Transf.* 68, 659 **(2014)**.
28. S. Han, L. Zheng, C. Li, and X. Zhang, *Appl. Math. Lett.* 38, 87 **(2014)**.
29. T. Salahuddin, M. Y. Malik, A. Hussain, S. Bilal, and M. Awais, *J. Magn. Magn. Mater.* 401, 991 **(2016)**.
30. M. K. Nayak, N. S. Akbar, V. S. Pandey, Z. H. Khan, and D. Tripathi, *Adv. Powder Technol.* 28, 2159 **(2017)**.
31. S. Mondal, N. A. H. Haroun, S. K. Nandy, and P. Sibanda, *Journal of Nanofluids* 6, 343 **(2017)**.
32. M. K. Nayak, A. K. Abdul Hakeem, B. Ganga, M. I. Khan, M. Waqas, and O. D. Makinde, *Computer Methods and Programs in Biomedicine* 186, 105131 **(2020)**.
33. M. K. Nayak, *Meccanica* 51, 1699 **(2016)**.
34. R. E. Bellman and R. E. Kalaba, *Quasilinearization and nonlinear boundary-value problems.* Rand Corporation, Santa Monica, CA, **1965**.
35. S. S. Motsa, *Journal of Applied Mathematics* 2013, 15 **(2013)**.
36. S. S. Motsa, P. G. Dlamini, and M. Khumalo, *Advances in Mathematical Physics* 2014, 12 **(2014)**.
37. I. S. Oyelakin, S. Mondal, and P. Sibanda, *Frontiers in Heat and Mass Transfer* 8, 1 **(2017)**.
38. A. Mishra, K. P. Priyadarsan, S. Mishra, and M. K. Nayak, *Heat Transfer-Asian Research* 50, 542 **(2020)**.